Pergamon

Int. J. Heat Mass Transfer. Vol. 38, No. 2, pp. 309–316, 1995

0017–9310/95 $9.50+0.00

0017–9310(94)00164–2

Heat transfer in injection moulding systems with insulation layers and heating elements

K. M. B. JANSEN

Faculty of Chemical Technology, Polymer Department, Delft University of Technology, PO Box 5045, 2600 GA Delft, The Netherlands

(*Received* 20 *July* 1992 *and in final form* 26 *April* 1994)

Abstract—An analytical model is derived and tested for heat transfer in injection moulding systems with coating layers or active heating elements attached to the mould walls. For this purpose a simple one-dimensional layer model was considered and convection and viscous dissipation contributions were neglected. A simple expression for the effect of the coating thickness and conductivity on the cooling time is derived. Further, the heating element model was tested with a specially designed heater cell. The measurements compare reasonably well with the predicted temperature response.

1. INTRODUCTION

Injection moulding is a flexible production technique for manufacturing complex-shaped, thin-walled polymer products, During this process a hot polymer melt is injected into the cavity where it solidifies upon cooling. This cooling process is crucial for both the material properties and the demoulding time. Low cooling rates generally result in lower thermal stresses and more relaxation of orientation, thus improving product quality, whereas for economical reasons high cooling rates are desired. Ideally, the mould wall temperature should be above the polymer solidification temperature during the injection stage and quickly drop below this temperature afterwards.

In the past various modifications for influencing the heat transfer of the standard injection moulding process were suggested. They may be classified into three major categories: (1) control of the heat transfer by means of the mould cooling fluid [1]; (2) use of a thin coating or a (locally) different mould material to elevate the contact temperature between melt and mould [2–6]; or (3) use of a heating element to actively regulate the cooling process [5–8]. The first proposal indeed was seen to be capable of improving the product quality [9], but is rather impractical since it involves the time-consuming heating and cooling of large parts of the mould system. The suggestion to use a thin coating is in fact the most elegant one, since it is most effective at the right time (during the filling stage) and at the right spot (near the mould wall, where the orientation level is highest). Several investigators indeed reported a decrease of the frozen-in orientation level when using these coatings [2, 4, 5]. Clearly, the last mentioned category (active heater) is the most promising one.

In this article the effects of a coating (Section 2) and heating elements (Section 3) on the heat transfer of injection moulding systems will be studied. Explicit expressions are derived, describing the temperature distributions and the effect of the coating thickness on the cooling time. The results derived for the coated mould wall are also applicable for the so-called in-mould-coating process. In this process a thin decorative sheet is applied to the mould walls, sticks to the subsequently injected polymer and is ejected from the mould as part of the finished product. In Section 4 heating curves, measured in the mould and directly at the heater surface, are compared with their predictions. Furthermore the effect of the heating elements on the relaxation of frozen-in orientation is briefly discussed.

2. HEAT TRANSFER WITH COATED MOULD WALL

During the filling stage of the injection moulding process conduction, convection and viscous dissipation may all influence the cooling behaviour, whereas in the subsequent holding and cooling stage, conduction predominates [10]. However, since this filling stage is significantly shorter than the total cooling time, only conduction contributions will be considered here. Further, for simplicity all thermal properties are assumed to be constant and heat effects due to solidification are neglected. The system essentially consists of several slabs of material, i.e. a hot polymer melt, a cold mould wall and a thin coating in perfect contact with this mould. Each of the layers is labelled with a number as is shown in Fig. 1. This number will be used in the subscripts to distinguish

NOMENCLATURE

a	thermal diffusivity, $\lambda/\rho c_p$
b	heat penetration coefficient, $\sqrt{\lambda \rho c_p}$
Bi	thermal resistance ratio, R_{23}/R_1
D_i	thickness of layer i
K_i	$(D_i/D_1)\cdot\sqrt{a_1/a_i}$
P_A	power per unit area [W m^{-2}]
Q_h	dimensionless source term, $P_A R_2/T^*$
R_i	thermal resistance, D_i/λ_i
R_{23}	R_2+R_3
$\tilde{t}$	dimensionless time, $a_1 t/D_1^2$
T_L	temperature due to passive layer
T_h	temperature due to heater
T_m	initial melt temperature
T_w	initial wall temperature
T^*	typical heater temperature rise, $P_A R_{23}$
$\tilde{T}_L$	dimensionless T_L, $(T_L-T_w)/(T_m-T_w)$
$\tilde{T}_h$	dimensionless heater temperature, T_h/T^*
$\hat{x}_i$	dimensionless thickness coordinate, x_i/D_i
$\tilde{x}_1$	$1-\hat{x}_1$.

Greek symbols

α_n	roots of $\alpha_n \tan \alpha_n = Bi$
ε_{ij}	$(b_i-b_j)/(b_i+b_j)$
λ	thermal conductivity
ρ	density
σ_{ij}	b_i/b_j
$\phi(\chi,\Omega)$	function of equation (18)
χ_i	$K_i\hat{x}_i/2\sqrt{\tilde{t}}$
Ω	$Bi^{-1}(1+\sigma_{14})\sqrt{\tilde{t}}$.

Subscripts

$i=1$	layer 1, polymer
$i=2$	layer 2, heater
$i=3$	layer 3, insulation
$i=4$	layer 4, mould
m	melt
w	wall.

between the different layers. Thus T_i, x_i and D_i denote the temperature, x-coordinate and thickness of layer i, respectively. Layer 2, the 'heater layer', will not be used until the next section. The dimensionless differential equation and initial conditions for each layer i are given by:

$$K_i^2 \frac{\partial \tilde{T}_i}{\partial \tilde{t}} = \frac{\partial^2 \tilde{T}_i}{\partial \hat{x}_i^2} \quad \tilde{T}_i(\hat{x}_i, 0) = \begin{cases} 1 & \text{if } i = 1, \\ 0 & \text{if } i = 2,3,4. \end{cases} \tag{1}$$

The coefficient K_i and the dimensionless temperature, time and thickness coordinate are given by:

$$K_i = \frac{D_i}{D_1}\sqrt{\frac{a_1}{a_i}} \quad \tilde{T} = \frac{T-T_w}{T_m-T_w} \quad \tilde{t} = \frac{a_1 t}{D_1^2} \quad \hat{x}_i = \frac{x_i}{D_i}.$$

Here a, T_m and T_w denote the thermal diffusivity, initial melt and wall temperature, respectively. Note that D_1 is taken as the half-thickness of layer 1. During the first instants of cooling both layer 1 and 4 may be treated as semi-infinite, resulting in the boundary conditions:

$$\tilde{T}_1(\hat{x}_1 \to \infty, \tilde{t}) = 1,$$
$$\tilde{T}_4(\hat{x}_4 \to \infty, \tilde{t}) = 0. \tag{2}$$

At the mould–coating and the coating–polymer interfaces, both temperature and heat flux are taken to be continuous. The solution of the three coupled differential equations with corresponding initial and

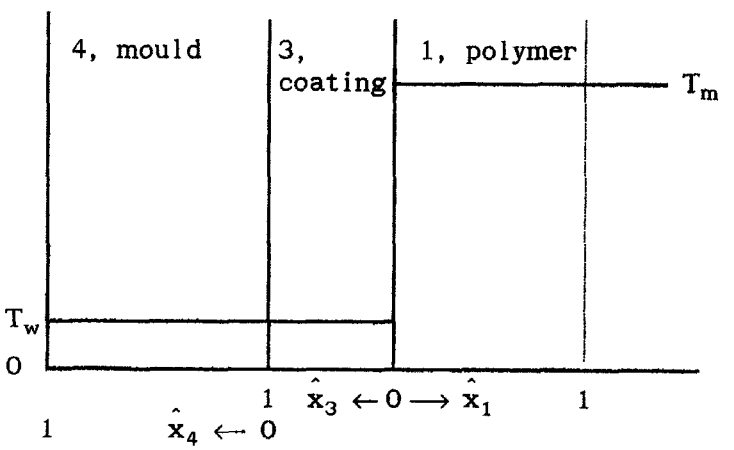

Fig. 1. System consisting of a hot melt layer (1), a coating (3) and a cold mould wall (4).

boundary conditions is obtained by using the standard Laplace transform technique [11]. This yields:

$$\tilde{T}_{1L} = 1 - \frac{1}{1+\sigma_{13}}\left\{\operatorname{erfc}[\chi_1] + \frac{2\sigma_{13}\varepsilon_{43}}{1+\sigma_{13}} \times \sum_{n=0}^{\infty}(-\varepsilon_{431})^n \operatorname{erfc}\left[\chi_1 + \frac{(n+1)K_3}{\sqrt{\tilde{t}}}\right]\right\}, \quad (3)$$

$$\tilde{T}_{3L} = \frac{\sigma_{13}}{1+\sigma_{13}}\left\{\operatorname{erfc}[\chi_3] - \varepsilon_{43} \times \sum_{n=0}^{\infty}(-\varepsilon_{431})^n\left(\operatorname{erfc}\left[\chi_3 - \frac{(n+1)K_3}{\sqrt{\tilde{t}}}\right] - \varepsilon_{31}\operatorname{erfc}\left[\chi_3 + \frac{(n+1)K_3}{\sqrt{\tilde{t}}}\right]\right)\right\}, \quad (4)$$

$$\tilde{T}_{4L} = \frac{2\sigma_{14}}{(1+\sigma_{13})(1+\sigma_{34})} \times \sum_{n=0}^{\infty}(-\varepsilon_{431})^n \operatorname{erfc}\left[\chi_4 + \frac{(2n+1)K_3}{\sqrt{\tilde{t}}}\right], \quad (5)$$

with

$$\chi_i = \frac{K_i \hat{x}_i}{2\sqrt{\tilde{t}}}, \quad b = \sqrt{\lambda\rho c_p}, \quad \sigma_{ij} = \frac{b_i}{b_j},$$

$$\varepsilon_{ij} = \frac{b_i - b_j}{b_i + b_j}, \quad \varepsilon_{431} = \varepsilon_{31}\cdot\varepsilon_{43}.$$

Here b and $\operatorname{erf}[\chi]$ denote the so-called 'heat penetration coefficient' and the complementary error function [12]. Note that the subscript 'L' is added to distinguish these solutions from the solutions in the next section.

The solutions above remain valid until the heat penetrates to the centre of the polymer slab ($\hat{x}_1 = 1$) or the mould wall ($\hat{x}_4 = 1$). These situations are reached for $t > 0.1D_1^2/a_1$ (about 1 s in case of a typical injection moulding situation) and $t > 0.1D_4^2/a_4$ (about 30 s), respectively. For small $\hat{x}_1$, the melt temperature may be approximated by equation (3) with $n = 0$. The error then remains below 1%, provided $\hat{x}_1 \leqslant 0.2$ and $\tilde{t} \leqslant 0.2$.

In the case of injection moulding the equations further simplify since the mould wall (layer 4) is a much better conductor than layer 1 (polymer) and does not yet influence the heat transfer of layer 1 and 3 during the first instants of cooling. Equations (3) and (4) are then completely governed by their first error function terms. The dimensionless contact temperature between layer 1 and 3, $\tilde{T}_{c13}$, is then constant and equal to:

$$\tilde{T}_{c13} = \sigma_{13}/(1+\sigma_{13}). \quad (6)$$

Note that if layers 1 and 3 have comparable thermal properties (as is the case with the heating elements described in Sections 3 and 4) $\sigma_{13} \approx 1$ and hence $\tilde{T}_{c13} \approx 0.5$.

For $t > 0.3D_3^2/a_3$, the heat starts to penetrate into layer 4 and $\tilde{T}_{c13}$ will decrease. Usually this initial stage is very short (about 0.01 s). For $t > D_3^2/a_3$, the transients in layer 3 vanish, resulting in a linear temperature profile, the slope and level of which still change with time. Furthermore, the contact temperature between layer 3 and 4 then becomes constant and equal to:

$$\tilde{T}_{c34} = \sigma_{14}/(1+\sigma_{14}). \quad (7)$$

Usually we have $\sigma_{14} \approx 0.05$, indicating that the contact temperature is only slightly higher than the initial mould temperature.

As was stated before, the model above fails as soon as the assumed boundary conditions are violated. Therefore an alternative model will be developed, suited for larger time-scales. Because of the symmetry, the boundary condition at the centre of layer 1 (i.e. at $\hat{x}_1 = 1$) becomes:

$$\frac{\partial \tilde{T}_1}{\partial \tilde{x}_1} = 0 \text{ at } \tilde{x}_1 = 0 \text{ with } \tilde{x}_1 = 1 - \hat{x}_1.$$

For convenience $\tilde{x}_1$ is used instead of $\hat{x}_1$ in the derivation below. Secondly, since the temperature in layer 3 turned out to be linear for larger times, the heat flux at the surfaces of layer 1 is proportional to the temperature difference over layer 3:

$$\frac{\partial \tilde{T}_1}{\partial \tilde{x}_1} = -Bi[\tilde{T}_1(t) - \tilde{T}_{c34}] \quad \text{at } \tilde{x}_1 = 1,$$

with

$$Bi = \frac{R_2 + R_3}{R_1} \quad R_i = \frac{\lambda_i}{D_i} \quad (\text{here } R_2 = 0). \quad (8)$$

Note that the Biot number, Bi, is defined as the ratio between the thermal resistance, R, outside and inside the polymer melt layer, which is analogous to the classical definition. For $\tilde{T}_{c34}$ we may use the value obtained from equation (7). Admittedly, this temperature should decrease with time due to the finiteness of layer 1 and 4. However, since σ_{14} is small, $\tilde{T}_{c34}$ tends towards zero and its effect on the temperature distribution in layer 1 may safely be neglected.

The set of equations and boundary conditions thus reduces to a standard problem with the following solution [11, p. 121]:

$$\tilde{T}_{1L} = \sum_{n=1}^{\infty} A_n \cos[\alpha_n \tilde{x}_1] \exp(-\alpha_n^2 \tilde{t}), \quad (9)$$

with

$$A_n = \frac{4\sin(\alpha_n)}{2\alpha_n \sin(2\alpha_n)} \quad \tilde{t} = \frac{a_1 t}{D_1^2}.$$

The roots α_n follow from the equation $\alpha_n \tan\alpha_n = Bi$, which can be solved conveniently for both small and large values of Bi. Here, the coating thickness is thin compared to that of the polymer layer and, since $\lambda_3 \approx \lambda_1$, $Bi \gg 1$. From a Taylor series expansion of α_1

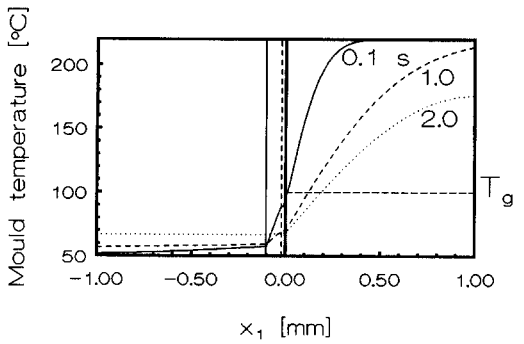

Fig. 2. Temperature distributions of a hot polystyrene sheet in contact with a cold, coated mould after 0.1, 1.0 and 2.0 s. The material properties and initial temperatures are listed in Table 1.

near $\pi/2$, it easily follows that:

$$\alpha_1 = \frac{\pi}{2}\frac{Bi}{Bi+1} + O\left(\frac{1}{Bi^2}\right),$$

and

$$A_1 = \frac{4}{\pi}\left[1 - \frac{\pi^2/8}{(1+Bi)^2}\right] + O\left(\frac{1}{Bi^3}\right).$$

Thus:

$$\tilde{T}_{1L} \cong \frac{4}{\pi}\left[1 - \frac{\pi^2/8}{(1+Bi)^2}\right]\cos\left[\frac{\pi}{2}\frac{Bi}{1+Bi}\tilde{x}_1\right] \times \exp\left[\frac{-\pi^2}{4}\left(\frac{Bi}{1+Bi}\right)^2\tilde{t}\right]. \quad (10)$$

The symbol $O(\ )$ is used to denote the order of magnitude of the remaining terms. In Fig. 2 some temperature profiles corresponding to real injection moulding conditions, calculated with equations (3)–(5), are plotted for $t = 0.1$ and 1.0 s, whereas equation (9) is used to calculate the temperature after 2.0 s of cooling. All relevant parameters are listed in Table 1.

In the injection moulding process it is important to keep the cooling time as low as possible and we will therefore try to estimate the influence of the coating layer on the cooling behaviour. The cooling time is here defined as the moment at which the polymer layer is completely solidified. Since the injection temperature is usually far above the solidification temperature (T_s), this cooling time is so large that equation (10) provides a fair approximation of equation (9). Inverting equation (10) with $\tilde{x}_1 = 0$ yields:

$$\tilde{t}_{c,L} \cong \left(1 + \frac{1}{Bi}\right)^2 \frac{4}{\pi^2} \ln\left[\frac{4}{\pi}\left(1 - \frac{\pi^2/8}{(1+Bi)^2}\right)\Big/\tilde{T}_s\right], \quad (11)$$

where $\tilde{t}_{c,L}$ denotes the dimensionless cooling time with a coating layer present. When compared with the cooling time without such a layer, $\tilde{t}_{c,0}$, the expression may be further simplified to:

$$\frac{t_{c,L}}{t_{c,0}} \cong \left(1 + \frac{1}{Bi}\right)^2 \quad \text{if } Bi \gg 1. \quad (12)$$

This expression thus gives the relative cooling time increment, which is a factor 1.2 for typical Bi values of about 10.

3. HEAT TRANSFER WITH ACTIVE HEATING ELEMENTS ATTACHED TO THE MOULD SURFACE

In this section the system as analysed so far will be extended with a thin heat producing layer attached to layer 3, in direct contact with layer 1. This heating layer may consist of an electrically conducting layer, uniformly heated by an electrical current. Layer 3 then serves as both an electrical and thermal insulation layer and will be largely responsible for the effectiveness of the heater as will be shown below.

The problem to solve is as follows. A hot polymer melt layer, initially at T_m, is on both sides in close contact with a heater layer (2), an insulation layer (3) and a mould wall layer (4), all initially at T_w. Then, after a certain delay time, layer 2 is heated with a uniform power density P_A during t_h s. Due to the linearity of the differential equations, this problem can be split up in a cooling part and a heating part. The cooling part is in fact very similar to the one treated in the previous section and may be solved in an analogous way. However, since in practice the heater layer (2) is thin and has a high thermal conductivity with respect to layer 3 (and 1), it will hardly affect the solutions. Thus the results of Section 2 may serve as an excellent approximation of the temperature field of the cooling part during the initial cooling period. The solutions for larger times are still given by equations (9) and (10), but now with $R_2 \neq 0$.

Table 1. Temperatures, thicknesses and thermal properties of the different heating element layers

Layer	Material	$T(t=0)$ (°C)	λ (W m^{-1} K^{-1})	ρ (g m^{-3})	c_p (J kg^{-1} K^{-1})	D (mm)	Source
1	Polystyrene	220	0.17	1050	1300	1.0	[12]
2	Carbon resin	50	1.41	1520	1510	0.025	Own
3†	PI (bulk)	50	0.375	1410	1340	0.087	Own
3‡	PI/PFA (4:3)	50	0.30	1730	1200	0.087	Own/[13]
4	Steel	50	15.0	7900	500	36	[14]

† Used for calculations in Sections 2 and 3.
‡ Mean values, corresponding to experimental situation (Figs. 5 and 6).

In the heating problem a source term is present in layer 2. For convenience, all initial temperatures are set to zero. What is calculated is in fact the temperature *difference* caused by the heating layer. The total temperature field then follows by simply adding the cooling part as given above. The differential equation and initial condition of layer 2 now become:

$$K_2^2 \frac{\partial \hat{T}_{2h}}{\partial \tilde{t}} = \frac{\partial^2 \hat{T}_{2h}}{\partial \hat{x}_2^2} + Q_h, \quad \hat{T}_{2h}(\hat{x}_2, 0) = 0, \qquad (13)$$

where Q_h denotes the dimensionless source term and the subscript 'h' is added for the sake of clarity. In all other layers this source term is absent. The temperatures are made dimensionless with T^*, the stationary temperature difference over layers 2 and 3 due to a heating power P_A: $T^* = P_A R_{23}$ (in analogy with the electrical voltage difference $V = IR$). The origin of the $\hat{x}_2$ coordinate is taken at the 1–2 interface.

The solution of this system of differential equations is straightforward but rather tedious. A quick calculation, however, shows that a 0.1 mm thick polymer coating at 100°C has an energy content of about 2 J cm^{-2} and will delay the heating process only about 0.1 s (if heated with 20 W cm^{-2}). Therefore, the heat capacity of layers 2 and 3 may be neglected. Assuming further that $T_{4h}(\hat{x}_4 \to \infty) = 0$ and $T_{1h}(\hat{x}_1 \to \infty) = 0$ and that the temperatures and fluxes at the interfaces are continuous, the system of equations finally yields:

$$\hat{T}_{1h} = \frac{2\sigma_{14}\Omega}{(1+\sigma_{14})^2} \text{ierfc}\,[\chi_1] + C_1 \phi(\chi_1 \Omega), \qquad (14)$$

$$\hat{T}_{2h} = \hat{T}_{1h}(\hat{x}_1 = 0, \tilde{t})$$

$$+ \frac{\hat{x}_2 R_2}{R_{23}} \left\{ \frac{\sigma_{14}}{1+\sigma_{14}} - \frac{\hat{x}_2}{2} + C_2 \,\text{erfc}\,[\Omega] \exp(\Omega^2) \right\}, \qquad (15)$$

$$\hat{T}_{3h} = \hat{T}_{2h} + \hat{x}_3(\hat{T}_{4h} - \hat{T}_{2h}), \qquad (16)$$

$$\hat{T}_{4h} = \frac{2\sigma_{14}\Omega}{(1+\sigma_{14})^2} \text{ierfc}\,[\chi_4] - \sigma_{14} C_1 \phi(\chi_4, \Omega), \qquad (17)$$

with

$$\Omega = \frac{1+\sigma_{14}}{Bi}\sqrt{\tilde{t}} \quad C_1 = \frac{1}{1+\sigma_{14}} - \frac{R_2}{2R_1}$$

$$C_2 = \frac{1}{1+\sigma_{14}} - \frac{R_2}{2R_{23}},$$

and

$$\phi(\chi, \Omega) \equiv \text{erfc}\,(\chi) - \text{erfc}\,(\chi + \Omega) \exp(2\chi\Omega + \Omega^2). \qquad (18)$$

Here ierfc denotes the integrated error function [12]. The function ϕ increases monotonically with time and ranges from zero to unity. Soon after the start-up, the second term of equation (18) vanishes and ϕ may be interpreted as a simple error function. The polymer surface temperature, $\hat{T}_{1h}(0, \tilde{t})$, then consists of a part which increases as the square root of time, and a part equal to C_1. This is exactly the kind of behaviour which was observed experimentally (see next section).

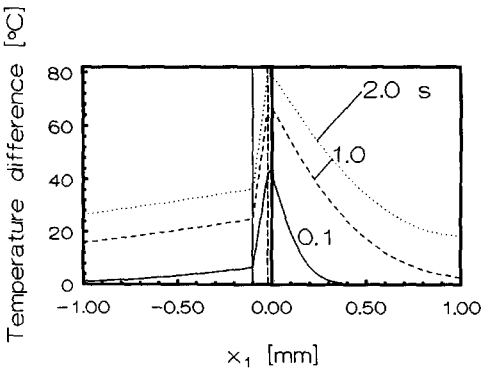

Fig. 3. Temperature distributions of cold polystyrene sheet in contact with an initially cold heating element after 0.1, 1.0 and 2.0 s of heating with 20 W cm^{-2}. Material properties as listed in Table 1; initial temperatures are set to zero.

An example of the (dimensional) temperature distributions after several periods of heating is given in Fig. 3. This clearly shows that the largest temperature rise occurs during the first half of a second. Further, after about 1 s, the heat starts to penetrate into the centre of the polymer slab. From then on the assumed boundary condition at $\hat{x}_1 = 1$ will be violated. The temperature should be higher, due to the heat pulse from the heater at the opposite mould wall, thus suggesting the first-order correction term of layer 1, $\hat{T}^c_{1h}$, to be:

$$\hat{T}^c_{1h}(\hat{x}_1, \tilde{t}) \cong \hat{T}_{1h}(2 - \hat{x}_1, \tilde{t}). \qquad (19)$$

4. HEATING EXPERIMENTS

On the basis of the principle given in Fig. 4, several heater cells were constructed. A steel block of $80 \times 35 \times 36$ mm^3 serves as a substrate for the heater layers. Parallel to the upper surface a 0.25 mm diameter chromel–alumel thermocouple was mounted. The thermocouple junction was only 0.13 mm below the surface. The insulation layer actually consisted of two polyimide (PI) layers, separated by PFA (fluoropolymer) glue. The ratio PI:PFA was 4:3. Furthermore, in contrast with the model system, used in Sections 2 and 3, a protective top layer of about 10 μm

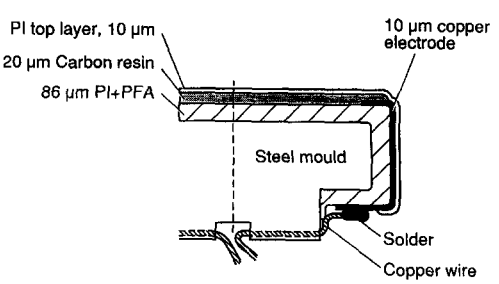

Fig. 4. Schematic representation of a heater cell with a thin thermocouple directly below the steel mould surface.

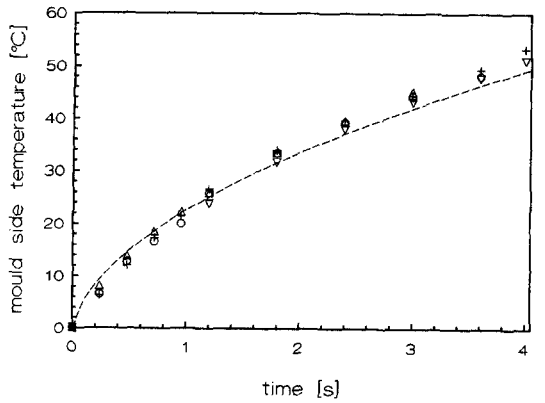

Fig. 5. Measured (symbols) and calculated (dashed line) mould temperature increments, during 4 s of heating and normalised to 20 W cm^{-2}. Experimental power densities of 11.6 (+), 14.9 (△), 15.5 (○) and 23.2 (▽) W cm^{-2}. Thermal properties and thickness as listed in Table 1.

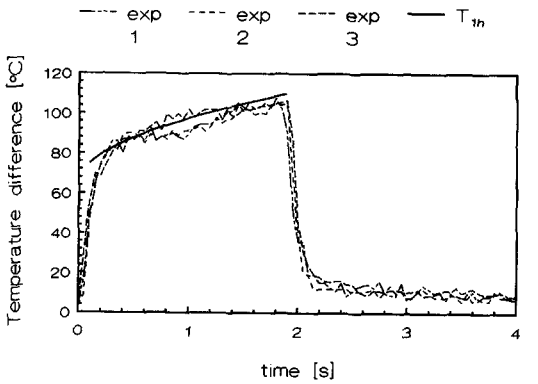

Fig. 6. Measured (dashed lines) and calculated (full line) surface temperature differences, for a heating pulse of 22.3 W cm^{-2} during 1.9 s. Thermal properties and thickness as listed in Table 1.

PI was added. The influence of this layer on the calculated and measured temperatures, however, may safely be neglected. A more detailed description of the heater construction is published separately [15].

The heating cells were tested in open air, i.e. without layer 1 present. Since the thermal penetration coefficient of air, b_1, is very small with respect to b_4, $\sigma_{14} \approx 0$ and equations (15) and (17) become in dimensional form:

$$T_{2h}(0,t) \cong P_A\left\{\frac{2\sqrt{t}}{b_4\sqrt{\pi}} + R_3\right\} \quad \text{for} \quad t > \frac{6D_3^2}{a_3}, \tag{20}$$

$$T_{4h}(\hat{x}_4,t) \cong P_A\left\{\frac{2\sqrt{t}}{b_4\sqrt{\pi}} - \hat{x}_4 R_4\right\}. \tag{21}$$

Note that the possible effect of free convection is not taken into account in equations (20) and (21). These equations, however, are still assumed to give an accurate estimate of the performance of the heater cells. As is shown by equation (20) the thermal conductivity (and thickness) of layer 3 can have a large influence on the heater temperature. This is important to realise since reported values of the thermal conductivity of PI vary between 0.12 and 0.37 W m^{-1} K^{-1}. Guarded hot plate measurements on PI bulk material, as performed at the Philips Research Laboratories, resulted in $\lambda_{PI}(35°C) = 0.375 \pm 0.002$ W m^{-1} K^{-1}. Although the conductivity determined on this bulk material may differ from that of foil material (used in the heater cell), the bulk conductivity value is used for all further calculations.

In Fig. 5 the temperature differences, measured with the thermocouple located in the mould block, are plotted. The different symbols correspond to different power densities used during the heating experiments. The temperatures are normalised to a power density of 20 W cm^{-2}. In doing so, all appear to coincide, giving one single curve. This indicates a complete linearity with respect to the power density, as was to be expected from equations (17) and (21). The predicted temperature curve of equation (21) is plotted as a dashed line. For this curve, the thermal properties as listed in Table 1 were used. The predictions agree fairly well with the measurements. However, for larger times the predictions are systematically below the experimental data. This could be due to the uncertainty in the thermal properties of the mould layer or the local deviations in heating power, due to slight fluctuations in the layer thickness.

The surface temperature was measured with an IR KT4 pyrometer (Heimann), aimed at a spot of 6 mm diameter, located in the centre of the heater surface. The emissivity was determined to be 0.83 ± 0.02. The temperature differences, caused by a heating pulse of 22.4 W cm^{-2} are plotted in Fig. 6. The experiment was repeated two more times, showing a typical measurement uncertainty of about 5°C. The full line represents the temperatures, predicted with equation (20). For $t > 0.2$ s, this corresponds well with the experimental temperatures, once more suggesting the correctness of the (average) thermal conductivity of layer 3 (if a value of $\lambda_3 = 0.20$ W m^{-1} K^{-1} was used instead of 0.30 W m^{-1} K^{-1}, the predicted temperature would have been 30°C higher). The initial overprediction might be caused by the instationary effects in layers 2 and 3 or the relatively low response time of the pyrometer (90% response in 0.1 s). After the heating period of 1.9 s a rather quick temperature drop is observed (not predicted by the model). This quick temperature decrease is very important for the practical application in injection moulding systems, since the effect of a heating element on the demoulding time should certainly not be large. The reason for the quick temperature drop is twofold. First of all, the heat capacity of the heater and insulation layers are very low and, secondly, due to the (relatively) high thermal conductivity of the mould, the mould temperature increase after heating was only about 30°C. Note that, for larger heating periods, the steel mould block will become saturated with heat, which will slow down the cooling process considerably.

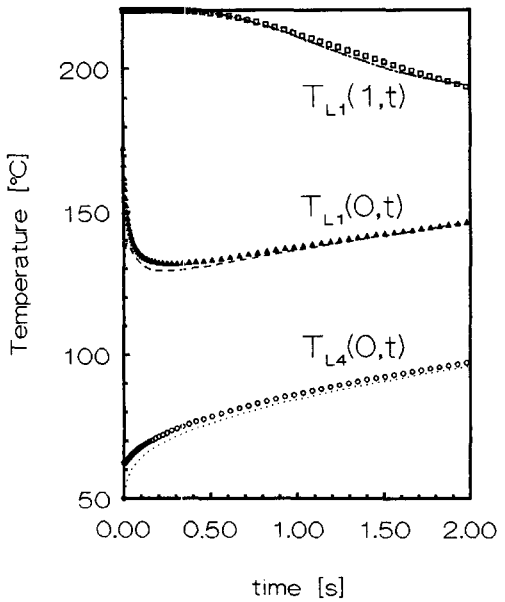

Fig. 7. Comparison between analytical (lines) and numerical (symbols) calculations. Initial temperatures as in Table 1 and heat source of 20 W cm^{-2} in layer 2. The heat capacity of layers 2 and 3 was neglected in both cases. $T_1(1,t)$, $T_1(0,t)$ and $T_4(0,t)$ denote the centre temperature of layer 1, the polymer–heater and mould–insulation layer interface temperature, respectively.

A fully implicit numerical model was used to verify the assumptions made. The properties and thicknesses are listed in Table 1. It turned out that neglecting the heat capacity of layers 2 and 3 caused the calculated temperature (T_L) to be about 3°C too high after 0.2 s. After 1 s the difference reduced to 1.7°C. From there on, a good agreement between numerical and analytical predictions was observed. In Fig. 7 the temperatures due to a combined heating (20 W cm^{-2}) and cooling (T_m = 220°C, T_w = 50°C) history are plotted. The lines and symbols denote the analytical and numerical approximations, respectively. The numerical approximation was performed with zero heat capacity of layers 2 and 3 and should therefore coincide with the analytical prediction. For small times ($t < 0.05$ s), however, this is clearly not the case, whereas for larger times the agreement is better. The reason for these discrepancies is not completely clear yet, although it is expected that they are partly due to numerical discretisation errors.

5. CONCLUSIONS AND FUTURE WORK

The present study aims to predict the polymer melt temperature in case of two modified injection moulding systems. In Section 2 the influence of a thin coating on the mould surfaces was investigated. The initial contact temperature is given by equation (6). For the injection moulding conditions of Table 1, this temperature increases from 50 to 112°C [equation (6)] if a polyimide coating is used. However, since the effect

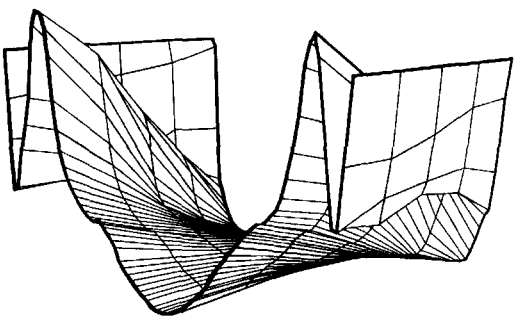

Fig. 8. Measured orientation distribution in injection moulded polystyrene strip. Moulding conditions as in ref. [16].

of the coating rapidly decreases with time, its application in real injection moulding systems might be rather limited. An active heating element on the other hand, provides a much more effective way of controlling the contact temperature. This idea is worked out in Section 3. The governing equations (14) and (17) are seen to agree reasonably well with experiments and with numerical calculations.

If the heating elements are applied during the injection moulding process, the temperature distribution in the polymer layer is simply obtained by adding the T_{1L} and T_{1h} terms. Using equations (10) and (14) this yields approximately:

$$T_{1,\mathrm{tot}}(x_1,t) \cong T_w + \frac{4}{\pi}(T_i - T_w)\left[1 - \frac{\pi^2}{8(1+Bi)^2}\right] \times \cos[\alpha_1 \tilde{x}_1]\exp(-\alpha_1^2 \tilde{t}) + \frac{P_A}{1+\sigma_{14}} \times \left\{\frac{2\sqrt{t}}{b_4\sqrt{\pi}} + R_{23} - \frac{\sigma_{14}}{\lambda_1}x_1 + \ldots\right\}, \quad \alpha_1 \cong \frac{\pi}{2}\frac{Bi}{Bi+1}. \tag{22}$$

The dimensionless ratio $P_A R_{23}/(T_i - T_w)$ expresses the (approximate) strength of the heating element relative to the initial temperature difference between melt and mould. This ratio can be used to estimate the power density necessary in a certain injection moulding situation.

To summarise all previous conclusions:

- an analytical model was derived which describes the temperature profiles in an injection moulding system with an insulation layer and a heating element attached to the mould wall;
- the assumption that the heat capacities of the insulation and heater layer may be neglected results in an overprediction of the surface temperature of 2–3°C only;
- the analytical predictions compare reasonably well with numerical calculations and experimental data;
- the relative increase in cooling time is given by a simple expression [equation (12)].

As was said in the introduction, the main objective

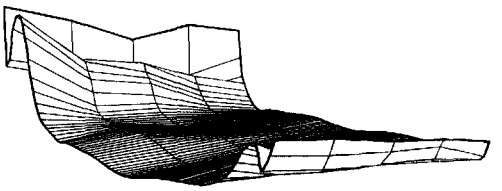

Fig. 9. As Fig. 8 but with a heating pulse of 2 s, applied directly after the filling stage.

for developing the heating elements was to enhance orientation and stress relaxation (and thus improve the product quality) in injection moulding. Therefore the heating elements were mounted in the rectangular mould ($80 \times 35 \times 2$ mm^3) of a 35-ton Arburg machine. The hydraulic pressure signal was used to trigger the heating pulse. All relevant signals were recorded by a data acquisition system. PS 678E (Dow) was used as an injection moulding material. The standard processing conditions were $T_i = 220°C$, $T_w = 50°C$, injection flow rate of 7.62 cm^3 s^{-1}, packing pressure of 700 bar and holding (cooling) time of 15 (30) s. This resulted in an orientation (or better, birefringence) distribution as depicted in Fig. 8. A heating pulse of only 2 s, applied just after the filling stage, results in a much lower orientation distribution (Fig. 9). The peak maxima are about a factor of 3 lower, which can be seen as quite satisfactory. The fact that the distribution is no longer symmetric is caused by differences in heating strength between the 'right' and the 'left' mould wall heater. More details about these injection moulding experiments are given in ref. [16].

Acknowledgements—The author is much indebted to many people at the Philips Research Laboratories without whom the construction of the heating elements would not have been possible. Further, the author wishes to thank Dr A. A. M. Flaman for his useful comments to the experimental part and kindly supplying his numerical program code and G. E. M. Hannen for performing the guarded hot plate measurements. This research was part of the IOP PCBP program of the Dutch Ministry of Economic Affairs.

REFERENCES

1. U. Delphy and S. Wintergerst, Spritzgießen mit veränderlichen Werkzeugtemperature, *Kunststoffe* **62,** 209–211 (1972).
2. G. Wübken, Einfluß der Verarbeitungs Bedingungen auf der innere Struktur thermoplastischer Spritzgußteile . . . , Ph.D. thesis, Aachen (1974).
3. G. Menges, B. Horn, P. Mohren and G. Wübken, Spritzgußwerkzeuge met wärmedämmende Formnestbeschichtigungen, *Plast Verarbeiter* **25,** 279–285 (1974).
4. R. Wimberger-Friedl, Analysis of the birefringence distributions in compact disks of polycarbonate, *Polym. Engng Sci.* **30,** 813–820 (1990).
5. M. J. Liou, Minimizing residual stresses in molded parts, Ph.D. thesis, Massachusetts Institute of Technology, Massachusetts (1987).
6. A. A. M. Flaman, Build-up and relaxation of molecular orientation in injection moulding, Ph.D. thesis, Eindhoven University of Technology, The Netherlands (1990).
7. B. H. Kim and N. P. Suh, Low thermal inertia molding, *Polym. Plast. Technol. Engng* **25,** 73–93 (1986).
8. R. R. Wadhwa and B. H. Kim, Experimental results of LTIM. I Length of filling, *Polym. Plast. Technol. Engng* **27,** 509–518 (1988).
9. L. I. Johnson, *Modern Plast.* **40,** 111 (1963).
10. J. R. A. Pearson, *Mechanics of Polymer Processing*, Chap. 19. Elsevier, London (1986).
11. H. S. Carlslaw and J. C. Jaeger, *Conduction of Heat in Solids* (2nd Edn), Chap. 12.8, Oxford Science Publications. Clarendon Press, Oxford (1988).
12. D'Ans Lax, *Taschenbuch für Chemiker und Physiker*, Band 1, 3. Auflage, pp. 1–701. Springer Verlag (1967).
13. Documentation of supplier (Dupont Nemours).
14. Documentation of supplier (steel X6CrNi 18-10).
15. K. M. B. Jansen and A. A. M. Flaman, Construction of fast-response heating elements for injection moulding applications, *Polym. Engng Sci.* **34,** 194–197 (1994).
16. K. M. B. Jansen and A. A. M. Flaman, The influence of surface heating on the birefringence distribution in injection moulded parts, *Polym. Engng Sci.* **34,** 898–904 (1994).